Soft Matter

Accepted Manuscript

ROYAL SOCIETY OF CHEMISTRY

www.rsc.org/softmatter

Soft Matter

Dynamic Article Links ►

Cite this: DOI: 10.1039/c0xx00000x

www.rsc.org/xxxxxx

ARTICLE

Anions make the difference: insights from the interaction of big cations and anions with poly(N-isopropylacrylamide) chains and microgels.

Leonor Pérez-Fuentes[a], Carlos Drummond[b], Jordi Faraudo[*c] and Delfi Bastos-González[*a]

Received (in XXX, XXX) Xth XXXXXXXXX 20XX, Accepted Xth XXXXXXXXX 20XX
DOI: 10.1039/b000000x

Minute concentrations of big hydrophobic ions have the ability to induce substantial effects in soft matter systems, including novel phases in lipid layers, giant charge inversion in colloids and nanostructuration in polymer surfaces in contact with water. The effects are so strong that the term "softmatter disruptors" was coined to describe their deep impact on interfaces, which goes far beyond that found by using the classical ions considered in lyotropic (Hofmeister) sequences. In these effects, solvation thermodynamics plays a fundamental role. Interestingly, it is possible to obtain big hydrophobic cations and anions with almost identical size and structure (e.g. Ph_4B^-, Ph_4As^+), which only differ in their central atom. Here we employ different techniques (Molecular Dynamics (MD) simulations, electrophoretic mobility and Atomic Force Microscopy (AFM)) to demonstrate the dramatic differences in the interaction of Ph_4B^- and $Ph_4As^+$with poly(N-isopropylacrylamide) (PNIPAM), a thermoresponsive polymer with expanded (well hydrated) and collapsed (poorly hydrated) states. Although both ions interact strongly with neutral PNIPAM chains and cationic or anionic PNIPAM microgels in the collapsed states, the effects of Ph_4B^- on PNIPAM are always substantially stronger than the effects of Ph_4As^+. MD simulations predict that ion-PNIPAM free energy of interaction is four times larger for Ph_4B^- than for Ph_4As^+. Electrokinetic and AFM experiments show that, acting as counter-ions, both ions are able to invert the charge of anionic or cationic PNIPAM microgels at minute concentrations, but the charge inversion due to Ph_4B^- is much larger than that obtained with Ph_4As^+. Therefore, even for big ions of identical size, shape and valence, the affinity of anions and cations for interfaces is intrinsically different.

1. Introduction

It is well known that ions with the same valence induce different behavior in a wide range of phenomena such as the surface tension of water electrolyte/air interface, effect of salt in colloidal stability, protein precipitation by salt, etc [1,2]. Although both cations and anions show these specific ionic effects, it has been known from long that anions show more pronounced specific ionic effects than cations [3–5]. This different behaviour has been attributed to the fact that anions are bigger and more polarizable than cations and these two variables play a major role in specific ionic effects [6]. It is also clear that anions interact with water in a different way than cations. Anions and cations have very different hydrogen bonding capabilities, as recognized in experiments of transfer of ions from solvents with different tendency to form hydrogen bonds but similar dielectric constant[7]. A recent classification of the most common monovalent and divalent ions in a 2D map with hydrophilicity and hydrophobicity as coordinates shows that cations are found near the "neutral" point (no substantial hydrophobic/hydrophilic character) whereas anions are spread further out, particularly so for the more hydrophobic region of the map[8]. It is worth noting that the relative hydrophobic or hydrophilic character of ions and interfaces is essential in understanding specific ionic effects [9,10].

Interestingly, MD simulations of hypothetical anions and cations identical in all respects except by the sign of the charge (i.e., equal size, charge, dispersion interactions) show that anions have more pronounced specific effects such as larger adsorption at the water/air interface[11] or larger adsorption at hydrophobic surfaces[12]. The simulations of these hypothetical ions also indicate that the ionic specific effects are directly linked to the ion-water interaction, which is different for cations and anions. The asymmetry between anions and cations of the same size arises because water molecules can approach closer to anions (due to the small size of the hydrogen atom) as compared with the cations (which interact with the larger oxygen atoms of water). Recent spectroscopy experiments clearly demonstrate the existence of this solvation asymmetry between anions and cations[13].

All these studies suggest that substantial insight in the difference between cations and anions could be obtained by considering real (instead of hypothetical) ions with (almost) identical size, valency and chemistry but differing only in their anionic or cationic character. This is precisely our objective in this article, by considering the interaction of the tetraphenyl ions Ph_4B^- and Ph_4As^+ (Figure 1) with a particular soft matter system (PNIPAM microgels). Both ions are large (their radius is about 0.5 nm[14,15]) and their external chemical and electronic structure is identical, with four phenyl rings responsible of the direct interaction of the ions with water, surfaces or interfaces. The anionic or cationic nature of the ions is due to the central atom (B or As), which does not interact directly with the environment (solvent or interfaces).

Minute concentrations of these big hydrophobic ions have the ability to induce substantial effects in soft matter systems. For example, they can induce novel phases in lipid layers[16], giant charge inversion in colloids[10,17] or induce nanostructuration in polymer surfaces in contact with water[18]. The effects are so strong that Leontidis et al.[16] coined the term "soft matter disruptors" to describe their deep impact on surfaces, which goes beyond what is observed for the classical ions considered in lyotropic (Hofmeister) sequences. It seems clear that in these effects, water structure[13] and solvation thermodynamics[10] play a fundamental role.

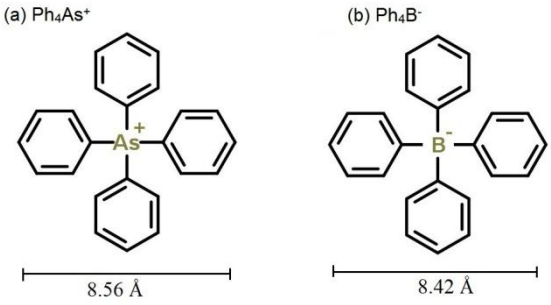

Fig. 1 Chemical structures of Ph_4As^+ and Ph_4B^- ions. The van der Waals diameter[15] is indicated.

We will consider here the interaction of these ions with a thermoresponsive polymer, PNIPAM (Figure 2a). This polymer undergoes a transition from extended coil to compact globule (or from swollen to collapsed states in the case of microgels) when the temperature is increased over a critical value —usually called lower critical solution temperature (T_{LCS})— which is around 31-34°C for PNIPAM[19]. According to previous studies with PNIPAM microgels[20] and PNIPAM charged chains[21], this system is particularly well suited for the study of specific ionic effects, due to its capacity to adsorb ions and its sensibility to the hydration state of ions. In addition, PNIPAM particles can be prepared with both cationic or anionic character, which allows the study of the behavior of ions Ph_4B^- and Ph_4As^+ as either counter-ions or co-ions.

In this paper, we show evidence from MD simulations, electrokinetic measurements and AFM imaging demonstrating dramatic differences between the specific effects due to the Ph_4B^- anion and the Ph_4As^+cation. The effects of Ph_4B^- on neutral PNIPAM chains and in cationic or anionic PNIPAM microgels are always much stronger than the effects of Ph_4As^+. We argue that the evidences provided here strongly support the view that even for big ions solvation of anions is essentially different than the solvation of cations and, more importantly, the affinity of anions and cations for interfaces is intrinsically different.

2. Materials and Methods

2.1 Chemicals

All the products used in this study were of analytical grade and used as received. N-Isopropylacrylamide (NIPAM), 2,2'-azobis(2-amidinopropane) dihydrochloride (V50), N, N-methylenebisacrilamine (MBA), aminoethyl methacrylate hydrochloride (AEMH) were obtained from Acros. Potassium persulfate (KPS), sodium chloride (NaCl), sodium tetraphenylborate ($NaPh_4B$), tetraphenylarsonium chloride (Ph_4AsCl) salts and polyelectrolyte polyethylenimine (PEI) were purchased from Sigma-Aldrich and Scharlau. Water was of Milli-Q quality.

2.2 Synthesis of PNIPAM microgels.

Anionic and cationic PNIPAM particles were prepared using batch radical polymerization. The cationic microgel was obtained following the protocol by López-León et al.[22] while for the anionic one we followed the protocol by Tagit et al.[23] . Polymerizations were performed in batchs of 500 ml for the cationic microgel and 350 ml for the anionic one, in a 1000 ml volume capacity reactor. The amounts of each reactant used are shown in Table 1. Negative charge on anionic microgels comes from sulfate groups supplied by KPS, while the positive charge on cationic ones comes from amino groups supplied by V50 and AEMH. Anionic microgels underwent three cycles of centrifugation/decantation/redispersion at 38°C at 14000 rpm (Kontron Instruments) for removal of unreacted material. On the contrary, it was not possible to deposit cationic microgels by centrifugation; instead, serum replacement was used for purification, until the conductivity of the samples was constant and close to the conductivity of Milli-Q water.

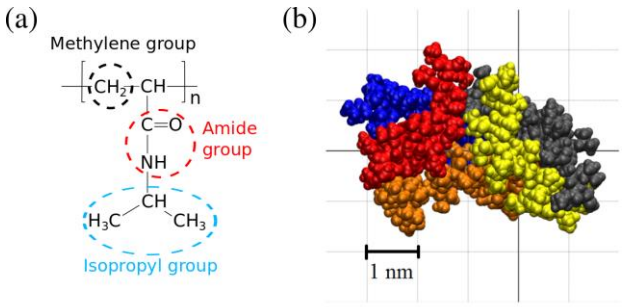

Fig. 2 (a) Chemical structure of PNIPAM. (b) Simulation snapshot of an aggregate made by the self-assembly of 5 PNIPAM chains at 45°C in presence of NaCl (simulation S2 in Table 2). Each PNIPAM chain is shown in a different color. Atoms are shown as spheres with their van der Waals radius. Water and ions are not shown for clarity.

2.3 Physicochemical characterization.

After the cleaning processes the diameter and the electrophoretic mobility of the microgels were investigated by dynamic light scattering (DLS) measurements using a Zetasizer Nano ZS (Malvern Instruments, UK). Data were obtained from the average of three measurements with a standard deviation lower than 5%. In addition, the morphology and the monodipersity of the microgels were analyzed by transmission electron microscopy (TEM) images (H-7000 FA Hitachi microscope).

2.4 Atomic force microscopy (AFM).

AFM experiments in liquid environment were carried out in tapping mode using SiO_2 tips on triangular Si_3N_4 cantilevers (NanoScope IV Multimode, Veeco Instruments, Santa Barbara, California, with a temperature control system Thermal Applications Controller). Freshly cleaved mica surfaces (Metafix, France) were used as the substrate for microgel adsorption. Mica is easily exfoliated, which makes it a perfect material to obtain clean surfaces that are smooth at the atomic level. Mica becomes negatively charged when it is submerged in water, so cationic components are readily adsorbed on it. The following experimental protocol was carried out: the tips were irradiated with ultraviolet light in a UV/ozone cleaner for 15 minutes prior to use.

Table 1. Amounts of each reactant used in the synthesis of the PNIPAM microgels.

	Water (ml)	NIPAM (g)	MBA (g)	KPS (g)	V50 (g)	AEMH (g)
Cationic	500	13.656	0.233	-	0.157	0.374
Anionic	350	4.9	0.49	0.291	-	-

Table 2. Summary of parameters for MD and MD-ABF computer simulations.

	T (K)	Number of Ions	Number of Water molecules	PNIPAM monomers	Total Atoms	Size Simulation box (Å)
S1 (MD)	298	15 Na^+ , 15 Cl^-	22248	100	68714	87.78
S2 (MD)	318	15 Na^+ , 15 Cl^-	22248	100	68714	87.78
S3 (MD)	318	15 Na^+, 15 Ph_4B^-	21779	100	67967	87.98
S4 (MD)	318	15 Ph_4As^+ , 15 Cl^-	22126	100	69008	88.47
S5 (MD-ABF)	318	1 Na^+, 1 Ph_4B^-	22365	100	69081	88.45
S6 (MD-ABF)	318	1 Ph_4As^+ , 1 Cl^-	22367	100	69087	88.46

Mica was glued on a steel disc and it was cleaved using adhesive tape immediately before use. For the case of anionic microgels, mica was coated with the cationic polyelectrolyte polyethylenimine (PEI) before microgel adsorption, in order to reverse the substrate charge and favour the adsorption of the anionic particles. For experiments in liquid environment we used a fluid cell sealed by a silicone O-ring, previously cleaned by rinsing with water and ethanol. Before adsorption, the device was heated at 38°C and a solution of diluted PNIPAM (previously heated at 40°C) was injected. In the case of the cationic (anionic) PNIPAM there is an electrostatic attraction between the mica (PEI-coated mica) surface and the microgel particles, which is enhanced when the microgel is in the collapsed state and its surface charge density is high. After one hour of adsorption, the liquid cell was rinsed with an unbuffered pH 4 solution (with HCl). After that, the desired salt solution (always at pH 4) was injected, and several images were taken at different temperatures. The temperature was decreased in steps of 2°C from 38°C until the phase transition of the microgel from the collapsed to the swollen state was observed (the final temperature depended on the salt employed). After that, the temperature was increased in steps of 2°C, until 37°C where the microgels were again in a collapsed state. In this way the temperature range was covered completely with precision of ± 1°C. The system was allowed to equilibrate for 15 minutes after each temperature change.

2.5 Methodology for Molecular Dynamics Simulations.

The MD simulation method is based on the numerical solution of the Newton equations of motion for all atoms of a molecular system constrained to the thermodynamic conditions (T, p). In our case, we have considered MD simulations of a solution containing neutral PNIPAM chains in water electrolyte with different combinations of ions (Na^+ and Cl^-, Na^+ and Ph_4B^-, Cl^- and Ph_4As^+). Before performing MD simulations, one needs to formulate an atomistic model for the system and its interactions. Here, intermolecular interactions were described by Lennard-Jones and Coulomb atom-atom interactions. Intramolecular interactions (bonds, angles, torsions, dihedrals,…) were described using the CHARMM27 force field [24,25]. In the case of PNIPAM chains, the parameters for the force field were the same employed in other simulations of PNIPAM[26,27]. For water, we employed the rigid TIP3P water model specified in standard CHARMM27 force field. For the Na^+ and Cl^- ions, we employed standard CHARMM27 parameters. In the case of Ph_4B^- and Ph_4As^+ ions, we employed the force field parameters developed in ref.[28], obtained from ab initio calculations (partial charges for each atom are also given in table SI-T2 in the Supporting Information). As seen in Figure SI-4 in the Supporting Information, the most important difference between the two ions is the charge of the central atom (As or B), which is the most charged atom of each ion. The partial charges of the external atoms of two ions are very similar and they have low values. All the MD simulations were performed using the VMD[29] and NAMD2 software[30] CUDA version 2.9. The Newton equations of motion were solved with a time step of 2 fs and electrostatic interactions were updated with a 4 fs time step. All bonds between heavy atoms and hydrogen atoms were maintained rigid. The nonbonding Lennard-Jones interactions were cut off at a distance of 1.2 nm employing a switching function starting at 1.0 nm. The particle Ewald summation method was employed with a 1 Å resolution. We employed periodic boundary conditions in all directions. The thermodynamic temperature was maintained constant (at 25°C or 45°C depending on the simulation) using a Langevin thermostat with a relaxation constant of 1 ps^{-1}. The pressure (1 atm) was maintained using the Nosé-Hoover-Langevin piston as implemented in NAMD with an oscillation period of 100 fs and a decay time of 50 fs. In all our simulations, we have considered a system containing 5 PNIPAM chains in water electrolyte. Each PNIPAM chain has 20 monomers and the terminal monomers were capped with a $–CH_3$ group, as in previous work[26]. The different ionic compositions, size of the system and other details considered in our simulations are summarized in Table 2. In each of these simulations, we randomly place the 5 PNIPAM chains, the ions and water. After energy minimization, we performed a NPT run between 80 and 90 ns, to ensure that slow magnitudes such as the polymer radius of gyration equilibrate. In the case of Ph_4B^- and Ph_4As^+, we have computed the Gibbs free energy characterizing the ion adsorption by performing additional simulations (S5 and S6 in Table 2). We started from the results of the previous simulations (S3 and S4 in Table 2) and removed all ions except one adsorbed ion and one counter-ion. We added more water, and performed further NPT runs (of about 30 ns). Once the system was again equilibrated, we

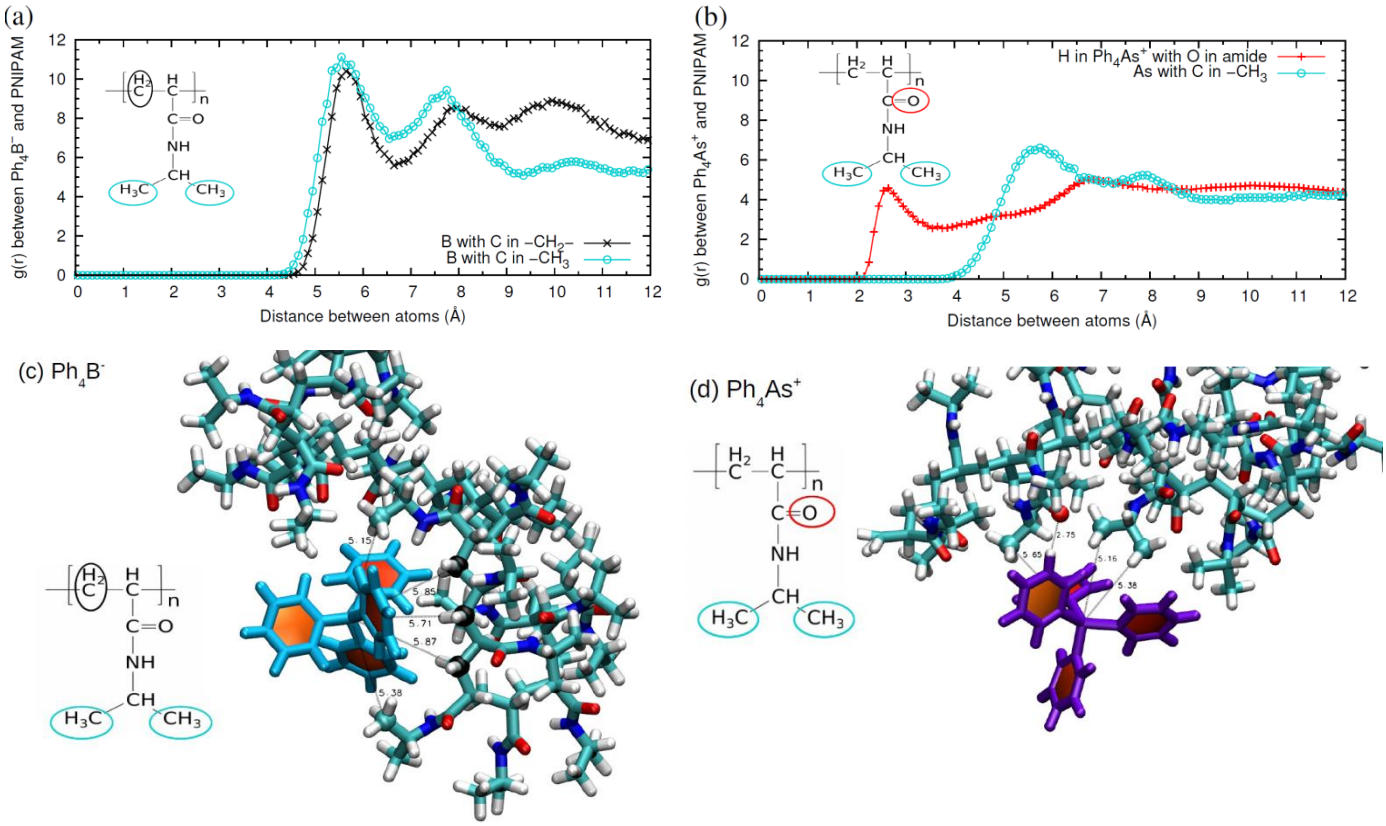

Fig. 3 Simulation results for the adsorption of ions on PNIPAM: atomic radial distribution functions g(r) and simulation snapshots indicating typical ion-PNIPAM distances contributing to the peaks of the g(r) functions. In all panels, the structure of the PNIPAM monomer is shown with indication of the chemical groups involved in the interaction. (a) g(r) between the central B atom in Ph_4B^- and carbon atoms in $-CH_2$ and $-CH_3$ groups of PNIPAM (b) g(r) between the central As atom in Ph_4As^+ and carbon atoms in $-CH_3$ groups of PNIPAM and between hydrogen atoms in Ph_4As^+ and oxygen atoms in amide groups in PNIPAM. (c) Snapshot of a simulation of PNIPAM with Ph_4B^- and (d) Snapshot of a simulation of PNIPAM with Ph_4As^+. All atoms are shown as bonds representations and water molecules are not shown for clarity. Ph_4B^- is shown in blue, Ph_4As^+ in violet and atoms in PNIPAM are coloured using standard colours (red = O, blue = N, white = H, cyan = C) except C atoms in $-CH_2$ groups interacting with ions which are shown in black.

performed biased simulations employing the adaptive biasing force (ABF) methodology[31]. In these calculations, we obtained the free energy (potential of mean force) over the distance between the adsorbed ion and the polymer (usually called reaction coordinate) by applying a biasing force to the system (see the Supporting Information (SI) for all technical details).

3. Results and Discussion

3.1 Self-assembly of chains in presence of NaCl

In previous MD simulation studies, the temperature-induced transition in PNIPAM was studied, but only at the single chain level[26,27,32,33]. This means that in these studies only the transition between coil and globule in a single PNIPAM chain was investigated, but the expanded/compressed state of PNIPAM particles was not simulated.

In principle, the interaction of ions with a single chain may differ with the interaction with aggregates containing several chains. For this reason, in this paper we will consider the interaction with a PNIPAM nanoparticle or aggregate (described in full atomistic detail), made by the self-assembly of several PNIPAM chains (see Methods section for details). Let us consider first simulations S1 and S2 in Table 2, which correspond to a system with 5 PNIPAM chains of 20 monomers each in presence of NaCl at two different temperatures (below and above the experimental transition temperature). A snapshot of a typical aggregate is shown in Figure 2b.

In both simulations, we observe aggregation of the PNIPAM chains after a few ns of simulation. However, the nature of the aggregates is very different at each temperature. In simulation S1 (25°C, below the transition temperature) the assembly is less stable, in the sense that partial disaggregation is sometimes found (i.e. a chain leaves the particle) and the size of the aggregate shows large fluctuations: the average radius of gyration of the self-assembled nanoparticle is Rg~ 2.5 nm but the system explores configurations with larger radius (~3 nm or more) or configurations with groups of smaller aggregates (~2 nm) during time intervals of the order of tens of ns. On the contrary, in simulation S2 (45°C, above the experimental transition temperature) we observe self-assembly of the chains onto a single aggregate or particle (cf. Figure 2b) with a radius of gyration Rg = 1.5 nm (with no significant fluctuations), consistent with a collapsed state. The expanded state obtained in simulation S1 is also more hydrated than the collapsed state obtained in S2, as expected (see SI for details). In both cases, the PNIPAM nanoparticle shows no adsorption of Na^+ or Cl^-. The analysis of the radial distribution functions g(r) presented in the SI shows that the Na^+ cation interacts with PNIPAM through the oxygen atom of the amide group, in agreement with previous results obtained for a single chain[27], although the interaction is not strong enough to lead to adsorption of Na^+. Concerning the anion, we did not observe significant interaction of Cl^- with PNIPAM.

3.2 Interaction of big hydrophobic ions with a PNIPAM hydrophobic nanoparticle: MD simulations.

Now, let us focus on the results for the interaction of the big hydrophobic ions of Figure 1 with a PNIPAM nanoparticle in the collapsed state (simulations S3 and S4 in Table 2). In analysing the results, it is important to keep in mind that the main difference between the two ions in the employed models is their anionic or cationic character due to the charge of the central atom (see model details in the Methods section and in the Supporting Information). The analysis of pair distribution functions (Figure 3) shows several remarkable features. First of all, it can be observed that both ions interact with the hydrophobic isopropyl group. In previous works[26], it was observed that poorly solvated anions (I^- and to a less extend Br^-) interact weakly with these groups. Here we see that this interaction is not exclusive to anions since both Ph_4B^- and Ph_4As^+ interact strongly with the isopropyl group. The driving force for this interaction can be clearly attributed to the hydrophobic effect. However, there are significant differences between g(r) obtained for each ion (compare Figures 3a and 3b). The first peak for the anion is more pronounced than the peak for the cation: the relative height is higher for the anion and it is broader for the cation, indicating that the anion-isopropyl interaction is stronger than the cation-isopropyl interaction. Interestingly, there is a clear secondary peak for the anion which is barely visible for the cation. This can be interpreted with the help of the snapshots shown in Figures 3c and 3d. As seen in Figure 3d, the cation tends to be adsorbed at the surface of the side chains of the PNIPAM aggregate, at distances around 5.16 Å – 5.65 Å of the different $–CH_3$ groups of the isopropyl moieties, giving rise to a peak in g(r) in Figure 3b. On the contrary, the anion tends to be engulfed by the PNIPAM chains, in contact with backbone methylene $–CH_2$- groups (at distances about 5.71 Å - 5.87 Å in Figure 3c) and $–CH_3$ groups of the lateral chains of PNIPAM. In this internal location, the anion cannot be in contact with both $–CH_3$ groups of a given isopropyl moiety, being only in contact with the $–CH_3$ group nearest to the backbone $–CH_2$- group. The direct contact with one of the $–CH_3$ of the isopropyl moieties gives the first peak in Figure 3a. The second peak in Figure 3a, located at about 7.75 Å, is due to the other $–CH_3$ group of the same isopropyl moiety, which is not in direct contact with the anion.

As we said, the engulfment of the Ph_4B^- anion by PNIPAM chains allows significant interaction of the ion with the methylene $–CH_2$- groups located in the chain backbone, as clearly seen in the g(r) shown in Figure 3a. A strong candidate for the driving force for this interaction is again the hydrophobic effect, which appears to be more important in the case of the Ph_4B^- anion than in the case of the Ph_4As^+cation. Also, we note that in previous studies[26,27] no interaction was found between the backbone of single PNIPAM chains and inorganic anions such as I^- and Br^-.

In Figure 3d we also see that the Ph_4As^+cation interacts with the oxygen atoms of the amide groups (cation hydrogen – PNIPAM oxygen distance 2.75 Å). The g(r) function between hydrogen atoms of Ph_4As^+ and amide oxygen atoms (Figure 3b) shows a clear peak corresponding to this ion – amide interaction. Previous works[27]show that the interaction of inorganic cations with PNIPAM amide groups is significant for small cations (such as Li^+) but it is weak for the largest cations (Cs^+) and it is also weak for hydrated divalent cations (Mg^{2+}, Ca^{2+}). We see here that the interaction is also present for this big hydrophobic cation. Therefore, the PNIPAM amide–cation interaction is not simply

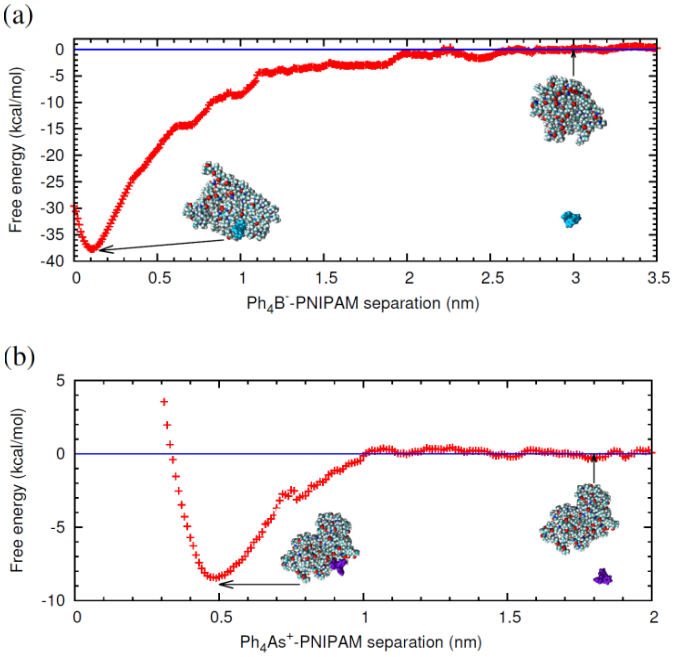

Fig. 4 Free energy (potential of mean force) corresponding to the interaction of (a) Ph_4B^- and (b) Ph_4As^+ with PNIPAM computed from ABF simulations S5 and S6 in Table 2.

determined by the size of the cation.The important factor is the ability to make bonds with oxygen atoms, which can be done either by a small cation (Li^+) with a large surface charge density or by a big molecular ion such as Ph_4As^+ which has many small hydrogen atoms able to interact with an interfacial oxygen atom. Therefore, our results in Figure 3 show that, although the hydrophobic effect plays a fundamental role in the interaction of both Ph_4B^- and Ph_4As^+ with PNIPAM, the structural details of the cation–PNIPAM or anion–PNIPAM interactions are different. The Ph_4As^+cation interacts with isopropyl and amide groups located in the side chains of PNIPAM and adsorbs onto the surface of the PNIPAM nanoparticle. On the contrary, the Ph_4B^- anion is able not only to adsorb onto the surface of the PNIPAM nanoparticle but it is also able to penetrate inside the PNIPAM nanoparticle.

We have also evaluated the strength of the interaction between PNIPAM chains and the Ph_4As^+ and Ph_4B^- ions using the MD-ABF simulations described in the Methods section (simulations S5 and S6 in Table 2). The results are shown in Figure 4. In the case of Ph_4B^- anion, the attractive interaction extends over a distance of about 1 nm and the minimum of the free energy shows the impressive value of -37.7 kcal/mol (expressed in units of thermal energy, this is -63.6 k_BT). In the case of the Ph_4As^+cation, the attractive interaction has a range of about 0.5 nm and the adsorption free energy is estimated to be -8.5 kcal/mol (-14.3 k_BT). The first important conclusion from these results is that the difference in the free energy of adsorption between the cation and the anion is very large, being the adsorption of Ph_4B^- more favorable than that of Ph_4As^+ by about 29 kcal/mol (i.e. by about 49k_BT). Interestingly, simulation results for the free energy of transfer of these ions from water to organic solvents[28] predict that transfer of Ph_4B^- is more favorable than transfer of Ph_4As^+ by a similar amount (between 24-40 kcal/mol depending on the models employed in the calculations). It is also interesting to note that in

Table 3. Microgel characterization. Hydrodynamic diameters (D_h) at 25°C and 51°C. Polydispersity index (PDI). Swelling ratios (S_w).Volumen phase transition temperature (T_{VPT}). Electrokinetic transition temperature (T_{ET}).

	D_h (25°C) (nm)	D_h (51°C) (nm)	PDI (51°C)	S_W	T_{VPT} (°C)	T_{ET} (°C)
Cationic	355 ± 10	206 ± 1	0.07 ± 0.01	5.1 ± 0.4	35.5 ± 0.2	38.7 ± 0.3
Anionic	629 ± 5	377 ± 5	0.06 ± 0.07	4.6 ± 0.2	33.5 ± 0.1	38.1 ± 0.2

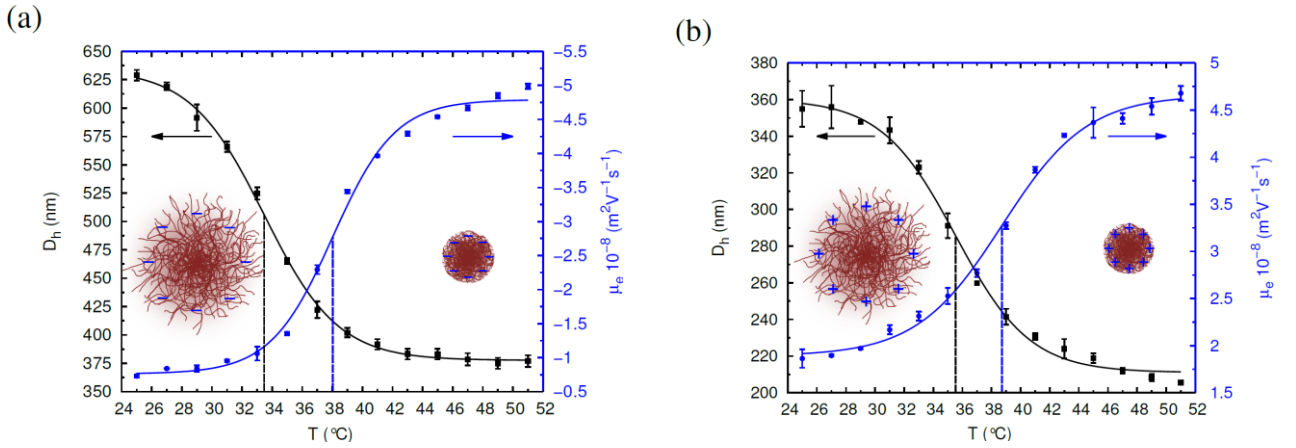

Fig. 5 Hydrodynamic diameter (■) and electrophoretic mobility, μ_e, (●) of the (a) anionic and (b) cationic PNIPAM microgels as a function of temperature at pH 4.

previous works it was observed that the energy of adsorption of Ph_4B^- onto cationic hydrophobic latex colloids was estimated to be larger than that for the case of Ph_4As^+ onto similar anionic latex colloids. The difference in free energy in that case was smaller[10,17], between 2-3 k_BT . We believe that the fact that the PNIPAM system is a soft, self-assembled particle plays a decisive role. In this case, the water surrounding the hydrophobic ions can be more efficiently removed and replaced by chemical groups of the polymer than in the case of adsorption onto a solid non deformable surface, in which at least two of the phenyl rings are completely immersed in water. Simulations performed in the case of a hydrophobic solid surface[34], show that adsorption of Ph_4B^- is preferred over adsorption of Ph_4As^+ by about 2.5k_BT. It is also remarkable that the interaction free energies obtained for the interaction of Ph_4B^- and Ph_4As^+ are much larger than the typical interaction energies of ions with interfaces. In the case of monovalent ions typical adsorption free energies[4] are of the order of a few k_BT and in the case divalent and trivalent ions with strongly charged interfaces (such as ionic lipid layers or membranes) we typically found[35,36] values of the order of 8-10k_BT. The strong interaction between Ph_4B^- and Ph_4As^+ with PNIPAM and the dramatic difference between both ions have substantial implications that can be experimentally observed, as will be explored in the next section.

3.3 Characterization of PNIPAM microgels.

Cationic and anionic PNIPAM microgels were produced as described in the Methods section. Once the microgels were purified, their main physicochemical properties were analyzed. First, the samples were studied by TEM to verify the monodispersity and sphericity of the particles (results shown in SI).Then the microgels were characterized in solution by DLS. The temperature dependence of the diameter and the electrophoretic mobility of the particles at pH 4 are shown in Figure 5. The diameters of both microgels progressively diminish around the volume phase transition temperature (T_{VPT}) when they transit from swollen to collapsed states. On the contrary, electrophoretic mobility values, μ_e, are very low when the particles are in the swollen state, due to high frictional forces[37], and progressively increase as the temperature surpasses the T_{VPT}. In addition, as the microgel shrinks its surface charge density increases, and this is reflected in higher mobility values.

The negative sign in μ_e confirms the nature of the anionic microgel (Figure 5a) while the μ_e positive values confirm the nature of the cationic one (Figure 5b). Table 3 shows the main data extracted from these figures. Anionic particles were bigger than the cationic ones. This can be justified by the presence of the charged AEMH co-monomer, besides the initiator, in the positive particles. During the polymerization reaction the presence of AEMH enhances the charge of the forming particles and for this reason the final particle size needed to stabilize the colloid is reduced. The low polydispersity index, PDI, obtained reflects a high monodispersity of both samples. The particle swelling ratios, S_W, were calculated from hydrodynamic volumes at 25°C and 51° C. Cationic particles showed a higher capacity of swelling than the anionic although the differences were not very significant. Table 3 also shows the transition temperature of the microgels obtained from the diameters, T_{VPT}, and the electrophoretic mobility,T_{ET}, calculated from the maximum of dD_h/dT and $d\mu_e/dT$ as a function of T, using a sigmoidal fitting. The T_{VPT} differences between both microgels can be explained taking into account that the cationic microgel incorporates the more hydrophilic co-monomer AEMH. As a consequence the temperature to transit from the swollen state to the collapsed one increases. On the contrary, the anionic microgel with NIPAM as unique monomer shows a lower T_{VPT} which is similar to that of PNIPAM chains[19].

3.4 Interaction of big hydrophobic ions with PNIPAM microgels: Electrophoresis.

The next set of experiments was aimed to analyse the role of the different salts on the electrophoretic mobility of the microgels. These results will allow us to compare how the electric state of the PNIPAM interface is changed depending on the nature of the ions present in solution. We have studied the two hydrophobic monovalent ions considered in the theoretical section, $Ph_4B^-(Na^+)$ and $Ph_4As^+(Cl^-)$ (see Figure 1). In addition, NaCl was used as reference salt, since according to our calculations previously described; we do not expect a significant interaction between NaCl ions and PNIPAM. The differences in the electrophoretic mobility observed in presence of the different salts can be ascribed to the hydrophobic ions. All the experiments were performed in unbuffered pH 4 solutions. The results are presented in Figure 6.

For the case of the anionic microgel (Figure 6a), Ph_4B^- anion acts as co-ion while Ph_4As^+cation acts as counter-ion. The ion specific influence of these two ions in comparison with NaCl becomes evident when we compare the electrophoretic mobility curves. These results reveal the accumulation of both ions at the PNIPAM-water interface, in agreement with the results of MD simulations for the uncharged PNIPAM chains. For the Ph_4B^- anion acting as co-ion, this accumulation is reflected in a substantial increase of the electrophoretic mobility in relation to NaCl at 1 mM, which is more evident as the microgel collapses and the surface becomes more hydrophobic. Note that the Ph_4B^- anion is electrostatically repelled from the anionic particle surface, but according to the calculations shown from results in Figure 4a, the free energy of interaction with PNIPAM is so strong (~-64 k_BT) that we expect a strong accumulation of Ph_4B^- onto the microgel even as a co-ion at very low concentrations (1 mM). For the Ph_4As^+cation, acting as counter-ion, the electrophoretic mobility almost vanishes at 1 mM of Ph_4As^+, and mobility inversion is readily observed when the concentration of cation is 10 mM. This mobility inversion is due to a charge reversal in the system: the Ph_4As^+ is being accumulated on the anionic microgel and the positive charge due to the adsorbed cation surpasses the anionic charge of the microgel; once again, this accumulation is more evident when the PNIPAM interface becomes more hydrophobic (i.e. at higher T).

Figure 6b shows the results for the cationic microgel. In this case, Ph_4B^- anion acts as counter-ion while Ph_4As^+cation acts as co-ion. The most striking result is the important inversion of the electrophoretic mobility observed with the Ph_4B^- at concentrations as low as 1 mM. The negative electrokinetic charge in presence of Ph_4B^- increases as the microgel collapse and it is even higher than the positive charge reached with the NaCl at 1 mM, (see Figure 6b). Hence, the charge reversal of the cationic PNIPAM is higher than 100%, which is an impressive figure. These results demonstrate an extremely large adsorption of Ph_4B^- onto hydrophobic PNIPAM particles in the collapsed state, in agreement with the strong adsorption of Ph_4B^- predicted in the previous calculations (Figure 4a). Figure 6b also shows the effect of Ph_4As^+ on the electrophoretic mobility of cationic microgels. In this case, the Ph_4As^+ acts as co-ion, and it is electrostatically repelled form the particle surface. However, according to previous calculations (Figure 4b), the free energy of interaction with PNIPAM (~-14 k_BT) is strong enough to overcome electrostatic repulsion and we expect an important accumulation of Ph_4As^+ onto the microgel. This predicted adsorption of Ph_4As^+ onto the cationic microgel is not reflected in the electrophoretic mobility reported in Figure 6a. There is almost no difference between the electrophoretic mobility in presence of $Ph_4As^+Cl^-$ or NaCl. As a plausible explanation we propose that the sum of the surface charge resulting from the accumulation of Ph_4As^+ and the cationic charge of the microgel is large enough to induce substantial condensation of the Cl^- counter-ions. This hypothesis is supported by AFM measurements reported in the next subsection.

As a summary of this subsection, the results shown in Figure 6a and 6b demonstrate that both hydrophobic ions (Ph_4B^- and Ph_4As^+) acting as counter-ions produce a large charge inversion in the microgels. This inversion is much more notable when the anion is acting as counter-ion. This stronger accumulation is reflected in higher electrophoretic mobility and lower concentration values at which the reversed charge is observed with Ph_4B^-. Therefore, we have provided a clear experimental demonstration that the two ions Ph_4B^- and Ph_4As^+ (which have the same size, shape and valence) have different interactions with an interface, being the anion the most active species, as predicted by our theoretical calculations (Figure 3).

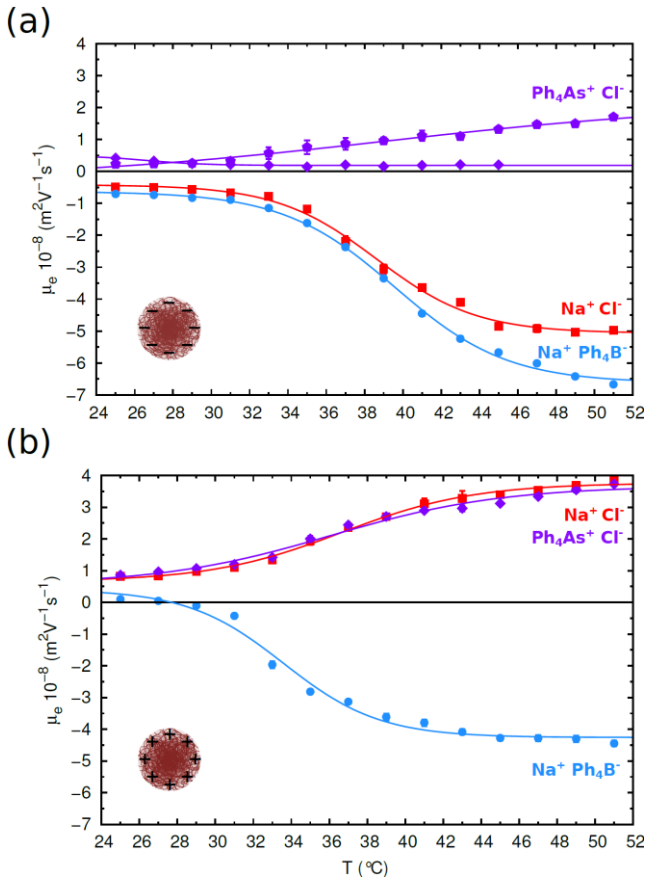

Fig. 6. Electrophoretic mobility, μ_e, of the (a) anionic and (b) cationic PNIPAM microgels as a function of temperature in presence of different salts and concentrations. (■) NaCl 1 mM; (●) $NaPh_4Cl$ 1 mM; (♦) Ph_4AsCl 1 mM; (⬟) Ph_4AsCl 10 mM.

3.5 Interaction of big hydrophobic ions with PNIPAM microgels: AFM.

The behavior of the adsorbed microgels was studied by tapping mode AFM using the procedure described above. AFM micro-

graphs were taken at several temperatures above and below the T_{VPT} of the microgels to analyze the effects produced by the accumulation of the hydrophobic ions on PNIPAM microgel particles. In order to simplify the discussion of the results only micrographs and height profiles for two temperatures, one above and one below the T_{VPT}, will be shown here.

Additional AFM micrographs taken at different temperatures are included as SI. Figure 7 shows the results obtained for the cationic and anionic microgels in presence of 1 mM of NaCl and with no added salt, respectively. For both microgels, it can be observed that when the particles are in the collapsed state they behave as hard particles; the individual particles can be clearly distinguished, as the edges of the particles are well defined. On the contrary, in the swollen state the particles are softer; as the AFM tip can penetrate them easily more blurred images are obtained, even though large tapping amplitudes were chosen in order to minimize the tip-substrate interaction. These differences can also be observed in the height profiles. At temperature above the T_{VPT} the individuality of the particles are reflected by well-defined, narrow peaks, while in the swollen state these peaks are wider, shorter and can even disappear reflecting the softer structure of the particles.

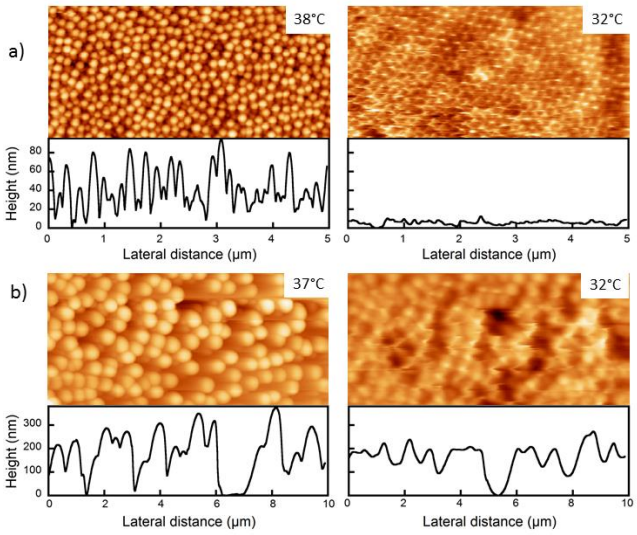

Figure 7. Height tapping mode AFM micrographs of the adsorbed PNIPAM microgels at two temperatures above and below T_{VPT} (a) cationic microgel; 1mM of NaCl; (b) anionic microgel at pH 4. A typical height profile for each sample is presented. The size of the images corresponds to the values shown in the horizontal axis.

Figure 8 shows the results obtained for the cationic microgel in presence of the two hydrophobic ions. As mentioned above, the PNIPAM particles were adsorbed on the mica surface from a solution of pH 4 before injection of the salts. In Figure 8a the micrographs obtained in presence of the anion Ph_4B^- at 1 mM are presented. Electrophoretic mobility measurements showed an important charge inversion when Ph_4B^- acts as counter-ion at this concentration. The ionic adsorption is also reflected in the AFM results. As the effective charge of the PNIPAM particles becomes negative they are not further attracted to the negatively charged mica surface. Therefore, as the tip scanned the surface, the particles were dragged along. The effect is more dramatic at low temperatures, when the pre-adsorbed hydrophilic particles are essentially removed from the surface by the rastering AFM tip. Figure 8b shows the results for the Ph_4As^+cation at 1 mM. In this case, because the cation is acting as co-ion, the accumulation on the surface of the PNIPAM increases the positive particle charge. Thus, the electrostatic interaction with the negatively charged mica is enhanced and the particles stay well fixed.

This is clearly reflected in the AFM images, which demonstrate the strong accumulation of this cation even acting as co-ion. From these data, our previous hypothesis to explain why we observed almost no differences on μ_e between this salt and NaCl appears more plausible. In order to further verify this accumulation we performed another experiment, by replacing the Ph_4B^- anion by the Ph_4As^+cation both at 1 mM, as shown in Figure 9. First, we scanned the surface in presence of the Ph_4B^- anion at 1 mM at different temperatures. We observed that many particles detached from the surface or formed aggregates (Figure 9a,b). Then, we washed the surface with pH 4 solution and after that we injected the Ph_4As^+cation at 1 mM and 38°C. As a result, the remained particles adhered again to the mica surface (Figure 9c; the images were taken in different areas of the sample).

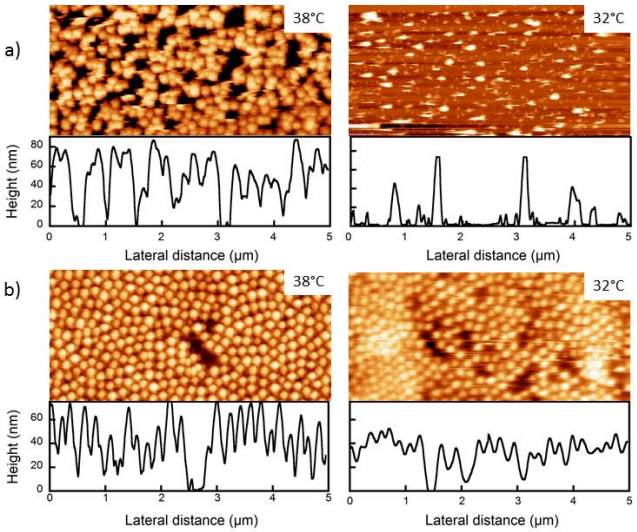

Figure 8. Height tapping mode AFM micrographs of the adsorbed cationic microgel at 1mM of (a) Ph_4B^- anion and (b) Ph_4As^+cation at two temperatures. A typical height profile for each sample is presented. The size of the images is shown in the horizontal axis of the profiles. The images at high temperature were taken few minutes after salt injection.

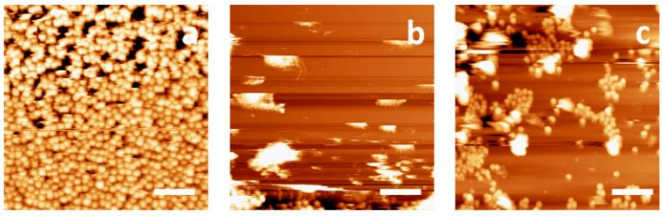

Figure 9. 5 μm × 5 μm height tapping mode AFM micrographs of the adsorbed cationic microgel. a) Scan right after injection of the Ph_4B^- at 1 mM; a different ordering of the particles can be observed between the beginning (lower section) and the end (upper section) of the image; b) image measured 6 hours after injection of Ph_4B^-; c) height image measured 4 hours after injection of Ph_4As^+at 1 mM. The scale bars correspond to 1 μm.

These results clearly evidence the accumulation of these two hydrophobic ions acting as counter- or co-ions. The experiments with the anionic microgel confirm these conclusions. Figure 10a shows the results in presence of Ph_4B^- anion at 1 mM. For this case, μ_e values showed an increase in the surface charge of the microgel due to the accumulation of Ph_4B^- acting as co-ion. AFM images show that even at 32°C particles are better attached to the surface than those corresponding at pH 4 (Figure 7b); the microgel particles appear better defined in presence of Ph_4B^-.

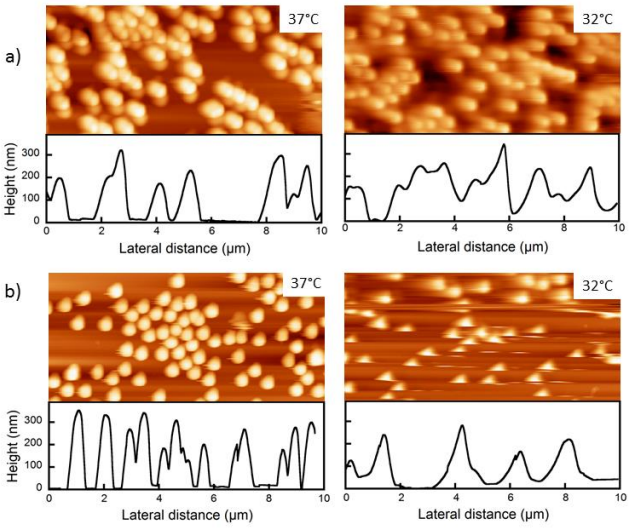

Fig. 10 Height tapping mode AFM micrographs of the adsorbed anionic microgel at 1 mM of (a) Ph_4B^- anion and (b) Ph_4As^+cation at two temperatures. A typical height profile for each sample is presented. The size of the images is shown in the horizontal axis of the profiles.

On the contrary, for the Ph_4As^+ cation at 1 mM, Figure 10b, AFM images show scanning-induced detachment of the particles at 32°C: only a section of some particles appear in the image. These results corroborate the charge inversion observed by μ_e with this cation acting as counter-ion. In addition, if we compare the images of Figure 8a and 10b, we can see that the detachment and the aggregation of the particles is higher when Ph_4B^- is acting as counter-ion than when Ph_4As^+ plays that role. This is also in agreement with the μ_e results, where we observed that the charge inversion was higher when Ph_4B^- anion was acting as counter-ion. It is also consistent with the MD results (Figure 4) in which we found higher affinity of PNIPAM for Ph_4B^- than for Ph_4As^+. In the broader context of specific ionic effects, our results could also have important implications in understanding why cations and anions play a different role in Hofmeister effects.

4. Conclusions

In this paper, we show evidence from MD simulations, electrokinetic measurements and AFM imaging demonstrating dramatic differences between the specific effects on a soft matter system (PNIPAM chains and microgels) of Ph_4B^- anion and the Ph_4As^+cation. Both molecular ions are almost identical in all relevant ion properties (size, surface groups interacting with materials, polarizability…) differing only in their anionic or cationic character. However, the effects of Ph_4B^- on neutral PNIPAM chains and in charged (cationic and anionic) PNIPAM microgels are always much stronger than the effects of Ph_4As^+.

The obvious question arising from these results is why apparently identical hydrophobic anions and cations have different interactions with soft interfaces in water. Correlation functions obtained from the MD simulations provide interesting clues. In previous works[11], it has been shown that in the case of identical anions and cations water molecules approach closer to anions due to the small size of the positively charged H atoms of water, leading to a higher disruption of water hydrogen bonding network by anions. The asymmetry in the anion-water hydrogen versus cation-water oxygen makes anions them more hydrophobic than cations of equal size[8,11,12]. Here, we observe a similar effect in the interaction of Ph_4B^- and Ph_4As^+ with interfaces, in this case PNIPAM chains. Both ions interact with the hydrophobic side chain $–CH_3$ groups (belonging to the isopropyl group) but according to the radial correlation functions obtained in our simulations (Figure 3) the Ph_4B^- anions are closer and interact more strongly than Ph_4As^+. Another difference observed in our simulations (Figure 3) is that Ph_4As^+ weakly interacts with amide groups in the side chains, whereas Ph_4B^-has a substantial interaction with $–CH_2$ groups present in the polymer chain backbone. All these evidences provided here strongly supports the view that even for big ions solvation of anions is essentially different than the solvation of cations and, more importantly, the affinity of anions and cations for interfaces is intrinsically different.

Acknowledgements

The authors wish to thank the financial support granted by the projects CTS-6270 (Junta de Andalucía, Spain) and MAT 2012-36270-C04-02 (The Spanish Government, Ministerio de Economía y Competitividad). We thank Red Española de Supercomputacion (RES) for computer time at the Minotauro Supercomputer (Barcelona, Spain) and technical assistance. We also thank Arturo Moncho-Jorda for useful comments on the manuscript draft. Carlos Drummond is specially indebt to the University of Granada (CEIBioTic 20F12/16) and Junta de Andalucía (IAC2/2011).

Notes

[a] *Biocolloid and Fluid Physics Group, Department of Applied Physics, University of Granada, Av. Fuentenueva S/N, E-18071 Granada (Spain).* *E-mail: dbastos@ugr.es*
[b] *CNRS, Centre de Recherche Paul Pascal (CRPP),UPR 8641, F3300, Pessac, France*
[c] *Institut de Ciència de Materials de Barcelona (ICMAB-CSIC), Campus de la UAB, E-08193 Bellaterra, Barcelona (Spain).*
E-mail: jfaraudo@icmab.cat
† Electronic supplementary information (ESI) available: Additional information on experimental and computational protocols.

References

1 W. (Editor) Kunz, *Specific Ion Effects*, World Scientific Publishing Co. Pte. Ltd., 1st Editio., 2009.

2 W. Kunz, *Curr. Opin. Colloid Interface Sci.*, 2010, **15**, 34–39.

3 J. Lyklema, *Fundamentals of Interface and Colloid Science*, Academic Press, London [etc.] :, 1991.

4 J. Lyklema, *Adv. Colloid Interface Sci.*, 2003, **100-102**, 1–12.

5 J. Lyklema, *Chem. Phys. Lett.*, 2009, **467**, 217–222.

6 D. J. Tobias, A. C. Stern, M. D. Baer, Y. Levin and C. J. Mundy, *Annu. Rev. Phys. Chem.*, 2013, **64**, 339–359.

7 Y. Marcus, *Chem. Rev.*, 2009, **109**, 1346–1370.

8 T. Morita, P. Westh, K. Nishikawa and Y. Koga, *J. Phys. Chem. B*, 2014, **118**, 8744–8749.

9 T. López-León, M. J. Santander-Ortega, J. L. Ortega-Vinuesa and D. Bastos-González, *J. Phys. Chem. C*, 2008, **112**, 16060–16069.

10 C. Calero, J. Faraudo and D. Bastos-González, *J. Am. Chem. Soc.*, 2011, **133**, 15025–15035.

11 L. Yang, Y. Fan and Y. Q. Gao, *J. Phys. Chem. B*, 2011, **115**, 12456–12465.

12 R. Zangi, *J. Phys. Chem. B*, 2009, **114**, 643–650.

13 R. Scheu, B. M. Rankin, Y. Chen, K. C. Jena, D. Ben-Amotz and S. Roke, *Angew. Chem. Int. Ed. Engl.*, 2014, **53**, 9560–3.

14 Y. Marcus, *Chem. Rev.*, 2007, **107**, 3880–3897.

15 J. I. Kim, *J. Phys. Chem.*, 1978, **82**, 191–199.

16 E. Leontidis, M. Christoforou, C. Georgiou and T. Delclos, *Curr. Opin. Colloid Interface Sci.*, 2014, **19**, 2–8.

17 A. Martín-Molina, C. Calero, J. Faraudo, M. Quesada-Pérez, A. Travesset and R. Hidalgo-Álvarez, *Soft Matter*, 2009, **5**, 1350.

18 I. Siretanu, J.-P. Chapel, D. Bastos-González and C. Drummond, *J. Phys. Chem. B*, 2013, **117**, 6814–6822.

19 H. G. Schild, *Prog. Polym. Sci.*, 1992, **17**, 163–249.

20 T. López-León, A. Elaïssari, J. L. Ortega-Vinuesa, D. Bastos-González and A. Ela"issari, *ChemPhysChem*, 2007, **8**, 148–156.

21 T. López-León, J. L. Ortega-Vinuesa, D. Bastos-González and A. Elaissari, *J. Colloid Interface Sci.*, 2014, **426**, 300–7.

22 T. López-León, A. Elaïssari, J. L. Ortega-Vinuesa and D. Bastos-González, *Chemphyschem*, 2007, **8**, 148–56.

23 O. Tagit, N. Tomczak, A. Jafarpour, D. Jańczewski, M. Y. Han, G. J. Vancso and J. L. Herek, *Nanotechnology*, 2011, **22**, 265701.

24 D. Yin and A. D. MacKerell, *J. Comput. Chem.*, 1998, **19**, 334–348.

25 J. B. Klauda, R. W. Pastor and B. R. Brooks, *J. Phys. Chem. B*, 2005, **109**, 15684–15686.

26 H. Du, R. Wickramasinghe and X. Qian, *J. Phys. Chem. B*, 2010, **114**, 16594–16604.

27 H. Du, S. R. Wickramasinghe and X. Qian, *J. Phys. Chem. B*, 2013, **117**, 5090–5101.

28 R. Schurhammer and G. Wipff, *J. Phys. Chem. A*, 2000, **104**, 11159–11168.

29 W. Humphrey, A. Dalke and K. Schulten, *J. Mol. Graph.*, 1996, **14**, 33–38.

30 J. C. Phillips, R. Braun, W. Wang, J. Gumbart, E. Tajkhorshid, E. Villa, C. Chipot, R. D. Skeel, L. Kalé and K. Schulten, *J. Comput. Chem.*, 2005, **26**, 1781–802.

31 J. Hénin, G. Fiorin, C. Chipot and M. L. Klein, *J. Chem. Theory Comput.*, 2010, **6**, 35–47.

32 S. A. Deshmukh, S. K. R. S. Sankaranarayanan, K. Suthar and D. C. Mancini, *J. Phys. Chem. B*, 2012, **116**, 2651–2663.

33 S. A. Deshmukh, G. Kamath, K. J. Suthar, D. C. Mancini and S. K. R. S. Sankaranarayanan, *Soft Matter*, 2014, **10**, 1462–80.

34 L. Pérez-Fuentes, D. Bastos-González, C. Drummond and J. Faraudo, (in preparation).

35 A. Martín-Molina, C. Rodríguez-Beas and J. Faraudo, *Phys. Rev. Lett.*, 2010, **104**, 3–6.

36 A. Martín-Molina, C. Rodríguez-Beas and J. Faraudo, *Biophys. J.*, 2012, **102**, 2095–103.

37 T. López-León, J. L. Ortega-Vinuesa, D. Bastos-González and A. Ela"issari, *J. Phys. Chem. B*, 2006, **110**, 4629–4636.